A Control System for Stable Operation of Autonomous Networked Microgrids

Mohsen Eskandari, Li Li, Mohammad H. Moradi, Fei Wang, Frede Blaabjerg, *IEEE Fellow*

***Abstract*—The interaction of droop controllers through power network is high in networked microgrids (NMGs) due to the low X/R ratio of the power lines impedance and lack of inertia in converter-based NMGs, which has raised stability concerns. On the other hand, inaccurate reactive power sharing and poor power quality due to the voltage and frequency deviations still remain as noticeable issues in NMGs. In this paper, a novel fuzzy consensus protocol is proposed to improve the droop controller performance in power sharing by incorporating the X/R ratio of the power lines impedance into droop loops. Power quality is also enhanced by restoring the average voltage profile based on a new consensus protocol, which is designed to be in coordination with reactive power sharing. In order to guarantee stability of the closed-loop system, linear matrix inequality method is adopted to determine the consensus signal coefficients as structured static output feedback gains. To this end, a novel small-signal model is proposed for NMGs to be adopted in the design process, by which the cross-coupling as well as interaction of droop controllers through the power network is properly realized. The numerical results in MATLAB/SIMULINK prove the effectiveness and accuracy of the proposed method.**

***Index Terms*—Dynamic Stability, Fuzzy Control, Microgrid, Power Sharing, Voltage Regulation, Output Feedback.**

I. Introduction

MICROGRID (MG) conceptually means the integration of distributed generation (DG) units into power systems with a suitable control strategy which enables local DG units and loads remain alive whenever the upstream network is not available [1]-[2]. Droop control is responsible for power sharing among DGs units as well as dynamic stability of MG, by which the MG designer is extricated from expensive and less reliable high band-width communication structures [3]-[6]. Despite of this considerable benefit, droop control performance significantly depends on the X/R ratio of the interconnecting power lines (feeder) impedance and does not provide accurate power sharing and secured dynamic stability for MGs. So, a complementary control strategy is needed to overcome the droop control drawbacks in power sharing and stabilization of MGs as well as a secondary controller to restore voltage and frequency deviations caused by droop controllers [4].

In this regards, the first wave of research took place mostly manipulating the droop control and evaluating its performance for MGs including parallel DG units [8]-[16]. Control strategies and related small signal models, presented in these works, consider simple MG architectures in which the DG units are connected to the MG bus at the point of common coupling (PCC), via power converters and feeder. However, MGs are located at the distribution level of power systems, normally with radial topology, while the parallel connection of DG units seems not to be very common in practical. On the other hand, the networked topology is more efficient due to a higher reliability [17], an improved voltage profile and less power losses compared to the radial configuration. Moreover, the networked topology enhances resiliency of the power systems [18]. To this end, second wave of research has been started by considering the control system performance in networked MGs (NMGs) [19]-[23]. Recently consensus control has been considered for accurate power sharing in NMGs. In this method, generation units reach a consensus, according to a protocol, which is defined based on the control target [20]-[24]. A comprehensive review of the consensus control and the required communication link including the communication delay/failure as the main obstacle of the consensus control is presented in [25]. However, still, there are some immature issues related to the basic consensus control in the content of NMGs which has not been thoroughly investigated. The major problems with the methods presented in the existing works in relation to the NMGs are listed as:

1) The stability analysis is overlooked since only the *V-Q* droop loop at an individual DG unit is analyzed. However, in NMGs with weak power networks, i.e. low X/R ratio, the interaction of droop controllers at generation nodes via the power network as well as cross-coupling effect between *f-P* and *V-Q* loops are dominant factors to specify the stability margin and dynamic performance of the system. This issue must be considered in the design process of the complementary/secondary controllers.
2) X/R ratio of the feeder impedance is not considered properly in the control system for the power sharing purposes. In particular, the power network in low voltage MGs is mostly based on cabling rather than overhead lines. As a result, the X/R ratio of power network impedance is around one, which makes the *f-P* and *V-Q* droop loops highly coupled. This is not desirable in terms of active and reactive power sharing since as it is investigated in this work *f-P* droop loop is in conflict with *V-Q* loop.
3) Voltage restoration is not addressed well, in order to be coordinated with *Q*-sharing. In these methods, the voltage magnitude at all generation nodes, is restored to a nominal value through an integrator at each node. On the other hand, an extra integrator is adopted per each node (for consensus protocol) to achieve precise reactive power sharing in an MG. However, voltage is a local variable in NMGs and

cannot be the same at all nodes. So the adopted rules for voltage restoration and reactive power sharing are in conflict and may put the system into an unstable region.

4) A systematic approach for consensus gains adjustment has not been proposed in order to achieve the desirable dynamic performance, while securing stability of the system.

Moreover, the frequently used small signal models, developed for a single VSI or parallel-based MGs, are not reliable in NMGs. The crucial issues with the parallel-based model is that the correlation between droop controllers is established via common reference frame (CRF) at the MG main bus [26]. The idea of CRF at the MG main bus, which is associated to the reference frame (RF) of a given droop controller, is not accurate in MGs, since there is no slack bus in MGs to regulate the frequency [27]-[28] and all droop controllers (not only a given one) are effective in the RF at the MG main bus. In other words, the MG main bus is not an infinite bus in the islanded MGs. As a result, the model is not accurate and the interaction of *f-P* and *V-Q* droop controllers through the power network is not appropriately modeled, which is highlighted and demonstrated in this work. In addition, effective elements, e.g. LC filter and VSI's inner loops, are not considered in some works, which reduces the accuracy of the model [29]-[30].

The contribution of this paper is as follows:

1) An accurate small-signal model is developed to evaluate the stability and performance of the droop control system in NMGs. In the proposed model, the interaction of droop controllers at NMG buses as well as the cross-coupling between *f-P* and *V-Q* droop loops is appropriately modeled.
2) Accurate active and reactive power sharing is achieved, regardless of the X/R ratio of the power lines in NMGs, by proposing a novel fuzzy-based consensus protocol.
3) A novel consensus algorithm is also proposed to restore the average voltage profile to the rated band by removing the droop control offset. The proposed consensus signals restore the voltage while maintaining accurate reactive power sharing.
4) The consensus gain determination is considered as a structured static output feedback problem, and consensus gains are designed by employing a linear matrix inequality (LMI)-based algorithm to solve the stabilization problem.

In the next section, the small signal model of the system is obtained. In Section III, novel fuzzy consensus protocols for power sharing and a consensus protocol for voltage regulation are introduced and the related parameters are adjusted. The simulation results are presented in Section IV, and finally conclusions are since in Section V.

II. NMG Control System Modeling

A. NMG Structure

The NMG architecture is depicted in Fig. 1. Each DG unit is composed of power converter interface and LC filter. NMG buses are connected to each other via the power network, consisting of low voltage 3-phase interconnecting power lines, in an arbitrary radial or meshed topology. Adjacent buses are linked by low band-width communication links.

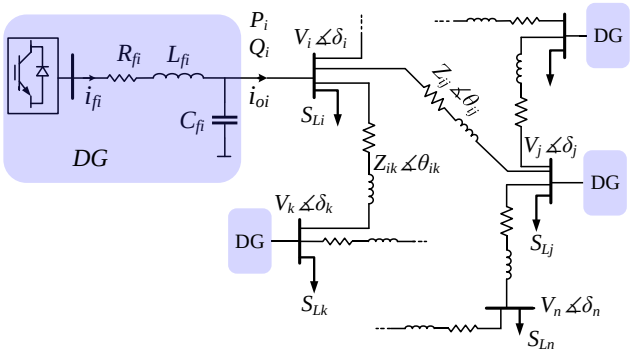

Fig. 1. An MG with a networked topology.

B. Power Flow Analysis

The active and reactive power (p and q) flowing from bus i to bus j, are given as:

$$\begin{bmatrix} p_{ij} \\ q_{ij} \end{bmatrix} = \frac{V_i}{Z_{ij}} \begin{bmatrix} V_i - V_j \cos(\delta_{ij}) & V_j \sin(\delta_{ij}) \\ -V_j \sin(\delta_{ij}) & V_i - V_j \cos(\delta_{ij}) \end{bmatrix} \begin{bmatrix} \cos(\theta_{ij}) \\ \sin(\theta_{ij}) \end{bmatrix} \quad (1)$$

Eq. (1) can be represented in the following form:

$$\begin{bmatrix} p_{ij} \\ q_{ij} \end{bmatrix} = \frac{V_i}{Z_{ij}} \left(\begin{bmatrix} V_i & 0 \\ 0 & V_i \end{bmatrix} - \Gamma(\delta_{ij}) \begin{bmatrix} V_j & 0 \\ 0 & V_j \end{bmatrix} \right) \begin{bmatrix} \cos(\theta_{ij}) \\ \sin(\theta_{ij}) \end{bmatrix} \quad (2)$$

$$where\ \Gamma(\delta_{ij}) = \begin{bmatrix} cos(\delta_{ij}) & -sin(\delta_{ij}) \\ \sin(\delta_{ij}) & cos(\delta_{ij}) \end{bmatrix},\ \delta_{ij} = \delta_i - \delta_j \quad (3)$$

Here i and j indexes denote the i^{th} and j^{th} buses. V & δ are the voltage magnitudes and phase angle, Z_{ij} & θ_{ij} are the magnitude and the phase angle of the ij^{th} interconnecting power line impedance. The following facts are reflected from the power flow equations presented in (1)-(3):

F1) Power flow through the power line is a function of the terminal buses variables, i.e. the voltage magnitude (V) and phase angle (δ);

F2) The interconnecting line impedance has great influence on the p and q flows. As it will be discussed later, it also causes cross-coupling effect between P and Q control loops;

F3) As per (3), in order to accomplish algebraic operation to the voltage magnitudes at terminal buses, e.g. bus i and bus j, at bus i, V_j is transformed to the RF of bus i, noting that $\Gamma(.)$ is a transformation matrix between two different RFs.

For each node the power balance equation would be:

$$0 = -p_i + \left(\sum_{j=1}^{n} \sigma_{ij} p_{ij} \right) + p_{Li} \quad (4)$$

$$0 = -q_i + \left(\sum_{j=1}^{n} \sigma_{ij} q_{ij} \right) + q_{Li} \quad (5)$$

where p_i and q_i are the injected active and reactive powers, respectively, p_{Li} and q_{Li} are local active and reactive loads, σ_{ij} is defined to be 1 if bus i is connected to bus j and 0 otherwise, and n is the number of NMG buses.

C. Small Signal Model

Droop control is widely adopted for power sharing among DG units in MGs. In this section, a novel small signal model, based on the power flow study, is proposed by which the interaction of droop controller as well as cross-coupling effect between *f-*

P and *V-Q* droop controllers is revealed. Moreover, the model accuracy is improved by adopting the local-based RF rather than the CRF.

1) Conventional droop controller:

The conventional *f-P* and *V-Q* droop controller rules [3] are given as:

$$\omega_i = \omega_0 - k_{pi} P_i \tag{6}$$

$$V_{refi} = V_0 - k_{qi} Q_i \tag{7}$$

where ω (ω_0) and V_{refi} (V_0) are the operating (nominal) angular frequency and voltage magnitude, respectively, k_p and k_q are the droop coefficients respectively, P and Q are average values of the output active and reactive powers, respectively. The i^{th} VSI's phase angle dynamic is given as:

$$\delta_i = \int \omega_i \, dt \;\Rightarrow\; \delta_i = \int \left(\omega_0 - k_{pi} P_i\right) dt \;\Rightarrow\; \delta_i = \omega_0 t + \int \left(-k_{pi} P_i\right) dt \tag{8}$$

Since ω_0 is the equilibrium frequency, $\int \left(-k_{pi} P_i\right) dt$ gives the phase variation around the equilibrium point, as described below:

$$\Delta \dot{\delta}_i = -k_{pi} P_i \tag{9}$$

The average active and reactive power are given by passing instantaneous output active and reactive power through a low pass filter (LPF) with the transfer function of $\omega_c/(s+\omega_c)$. Hence, the state variables of average active and reactive power are obtained as:

$$\dot{P}_i = -\omega_c P_i + \omega_c \left[\sum_{j=1}^{n} \left(\sigma_{ij} \, p_{ij}\right) + p_{Li} \right] \tag{10}$$

$$\dot{Q}_i = -\omega_c Q_i + \omega_c \left[\sum_{j=1}^{n} \left(\sigma_{ij} \, q_{ij}\right) + q_{Li} \right] \tag{11}$$

where ω_c is the cutting frequency of the low pass filter, p_{Li} and q_{Li} are the local bus load obtained by:

$$\begin{bmatrix} p_{Li} \\ q_{Li} \end{bmatrix} = \begin{bmatrix} v_{odi} & v_{oqi} \\ v_{oqi} & -v_{odi} \end{bmatrix} \begin{bmatrix} i_{Ldi} \\ i_{Lqi} \end{bmatrix} \tag{12}$$

where v_{odi} and v_{oqi} are the *d-q* components of the output voltage at the i^{th} DG unit, respectively, i_{Ldi} and i_{Lqi} are the *d-q* components of the local load current of the i^{th} DG unit, which are considered as disturbances in this paper.

2) VSI model

A VSI consists of the LC filter as well as inner voltage and current loops. The inner loops modify the LC filter dynamic to fix the VSI output voltage to the reference values coming from the power (droop) loop (13) and reject disturbances. The inner loops with faster dynamic than the power loop also compensate for the DC link voltage fluctuations caused by imbalance between the input and output power to the DC bus.

$$\begin{bmatrix} v_{odrefi} \\ v_{oqrefi} \end{bmatrix} = \begin{bmatrix} V_{refi} \\ 0 \end{bmatrix} \tag{13}$$

The VSI model is well developed in the literature [16], [20]. So for the sake of fluency of the paper, it is presented in the Appendix B.

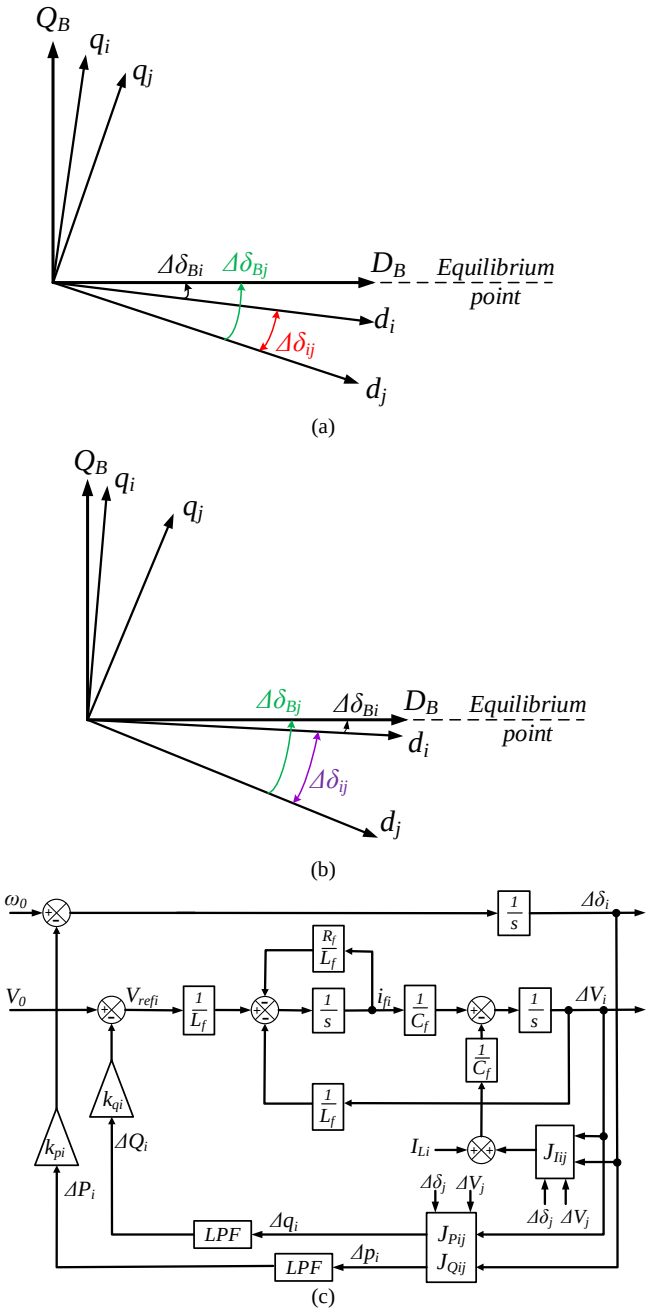

Fig. 2. Small signal representation of the droop control system in MGs: (a) small signal representation of reference frame in parallel-based MGs; (b) small signal representation of RF in parallel-based MGs including slack bus (bus *i*); (c) block diagram of the droop-based control system for the NMG given from the small-signal model.

3) Power network model considering interaction of the controllers

Highlight 1: when a disturbance is inserted into the power network, all power network variables, i.e. voltage magnitude and phase angle at network nodes as well as *P* and *Q* through power lines, are affected. As per **F1,** active and reactive power flows depend on the voltage magnitude and phase angle at terminal buses. On the other hand, droop controllers seek to alter the voltage magnitude and phase angle to control their output power (6)-(7). As a result, droop controllers insert other inputs to the power network. Specifically, the inputs, i.e.

changing voltage magnitude and phase angle, are based on the *P* and *Q* variations through the power network. In this way, droop controllers interact to each other via the power network. This interaction is high because of the low X/R ratio and lack of inertia in the droop-controlled converter-based NMG to smooth phase angle and voltage variations. Furthermore, as per **F2**, grid impedance relates *P* and *Q* variations to the voltage magnitude and phase angle (cross-coupling). Therefore, in order to model the interaction of droop controllers as well as the cross-coupling between *f-P* and *V-Q* droop loops, the variables by which the DG unit interacts with each other (i_{ij}, p_{ij} and q_{ij}) should be obtained in terms of the voltage magnitude and the phase angle at terminal buses, which are determined by droop controllers. To this end, assuming all signals at the same RF, the current in the ij^{th} power line ($Z_{ij}\angle\theta_{ij}$) is obtained as:

$$\begin{bmatrix} i_{dij} \\ i_{qij} \end{bmatrix} = \frac{1}{Z_{ij}} \Gamma\left(-\theta_{ij}\right) \begin{bmatrix} v_{odi} - v_{odj} \\ v_{oqi} - v_{oqj} \end{bmatrix} \tag{14}$$

where $\Gamma(.)$ operator is given from (3).

Highlight 2: As per **F3**, v_{odj} and v_{oqj} in (14) must be transformed to the RF of DG *i*, which is specified by the droop controller at this bus. In the conventional small signal model of parallel-based MGs presented in [26], variables of all parallel DG units are transformed to the RF at the MG bus, determined by a given *f-P* droop controller, which is called CRF. However, this model would be accurate if there is a large DG unit with zero or very small droop gain, responsible for the frequency regulation at the MG main bus, to make it as a slack bus with a fixed frequency. Nonetheless, this is not profitable in MGs regarding the small scale of DG units [27]-[28]. As a result, the CRF is not applicable in MGs and the model presented in [26] is not accurate as the effects of other droop controllers on the common RF are neglected. This issue is investigated in Fig. 2, which indicates the small-signal representation of the CRF in MG (please notice that the phase angle variation from the equilibrium point is represented ($\Delta\delta$), while the phase angle value and the phase angle dynamic at MG's main bus ($\Delta\delta_B$), which are negligible due to lack of droop controller in this bus, are ignored for the sake of clarity). Since the MG bus is represented in the CRF (DQ_B:=dq_i), $\Delta\delta_{ij}$ is adopted, instead of $\Delta\delta_{Bj}$, to correlate the state space model of VSI *j* to the MG's common bus which is not accurate. On the other hand, Fig. 2(b) shows the idea of the slack bus. Putting a large DG unit at bus *i* with zero or very small droop gain, limits the phase angle variation at bus *i* ($\Delta\delta_i$), which makes $\Delta\delta_{ij} \approx \Delta\delta_{Bj}$. However, the model developed based on CRF is not a precise model and, as mentioned earlier, it is not applicable in MGs due to small scale of DG units and current limits of the semiconductors.

In order to address this issue, motivated from the power flow equations, when the first order differential equations related to generation bus *i* are developed, the RF of bus *i* (the local RF) is regarded as base and the *d-q* components of voltage at bus *j* are transformed to the RF of bus *i* using the relevant transformation matrix, $\Gamma(\delta_{ij})$ in (3). Noting that the operator $\Gamma(.)$ satisfies $\Gamma(\delta) \times \Gamma(\theta) = \Gamma(\delta + \theta)$, (14) is updated as:

$$\begin{bmatrix} i_{ijd} \\ i_{ijq} \end{bmatrix} = \frac{1}{Z_{ij}} \left(\Gamma\left(-\theta_{ij}\right) \begin{bmatrix} v_{odi} \\ v_{oqi} \end{bmatrix} - \Gamma\left(\delta_{ji} - \theta_{ij}\right) \begin{bmatrix} v_{odj} \\ v_{oqj} \end{bmatrix} \right) \tag{15}$$

Finally, to obtain the small signal model of p_{ij} and q_{ij} in (10)-(11), we have:

$$\begin{bmatrix} p_{ij} \\ q_{ij} \end{bmatrix} = \frac{1}{Z_{ij}} \begin{bmatrix} v_{odi} & v_{oqi} \\ v_{oqi} & -v_{odi} \end{bmatrix} \left(\Gamma\left(-\theta_{ij}\right) \begin{bmatrix} v_{odi} \\ v_{oqi} \end{bmatrix} - \Gamma\left(\delta_{ji} - \theta_{ij}\right) \begin{bmatrix} v_{odj} \\ v_{oqj} \end{bmatrix} \right) \tag{16}$$

Adopting (15)-(16) i_{ij}, p_{ij} and q_{ij} are developed as function of voltage magnitude and phase angle (which are defined as state variables) at bus *i* and *j*.

4) Complete NMG Model

The state variables of NMG are defined as:

$$x_i = \Delta\left[\delta \;\; P \;\; Q \;\; \varphi_d \;\; \varphi_q \;\; \gamma_d \;\; \gamma_q \;\; i_{fd} \;\; i_{fq} \;\; v_{od} \;\; v_{oq}\right]_i^T, \;\; \forall \;\; i = 1:n \tag{17}$$

where φ_{dq} and γ_{dq} are the state variables related to VSI's inner loops (given in the Appendix B), $i_{f,dq}$ are the *d-q* component of the LC filter's inductor current. The small signal model of NMG is obtained as:

$$\dot{x}_i = \left[J_{ii} \;\; x_i + \sum_{\substack{j=1 \\ j \neq i}}^{n} \left(\sigma_{ij} \; J_{ij} \;\; x_j \right) \right] + B_i u_i + B_{Di} \left[\Delta i_{Ldi} \quad \Delta i_{Lqi} \right]^T, \; \forall i = 1:n \tag{18}$$

$$B_{Di} = \begin{bmatrix} 0 & \omega_c v_{odi0} & \omega_c v_{oqi0} & 0_{1\times6} & -1/C_{fi} & 0 \\ 0 & \omega_c v_{oqi0} & -\omega_c v_{odi0} & 0_{1\times6} & 0 & -1/C_{fi} \end{bmatrix}^T$$

$$B_i = \begin{bmatrix} 1 & 0_{2\times1} & 0 & 0 & 0 & 0 & 0 & 0_{3\times1} \\ 0 & 0_{2\times1} & 1 & 0 & k_{pv} & 0 & k_{pv}k_{pc}/L_f & 0_{3\times1} \end{bmatrix}^T$$

where J_{ii} and J_{ij} are the Jacobian matrices for the i^{th} DG unit (which are represented in the Appendix A), $u_i \in R^{2\times1}$ is input signal to the DG *i* control system to modify the droop controllers in (6)-(7) presented in the next section and B_i is its relevant input matrix, $\Delta i_{L,dqi}$ are the *d-q* components variation of the local load current as inputs, which are considered as a disturbance to the system, B_{Di} is the disturbance input matrix at bus *i*, k_{pv} and k_{pc} are control parameters of the VSI's inner loops given in Appendix B, L_f and C_f are LC filter's inductance and capacitance, respectively. The block diagram of NMG droop control system, derived from the developed small signal model, is depicted in Fig. 2(c), noting that VSI's inner loops and *q* component are ignored for the sake of clarity. It shows that the overlapping point of *f-P* and *V-Q* droop loops is the Jacobian matrix and $\Delta\delta$ and ΔV of the adjacent droop controllers appear in the closed loop control system to model the interaction of droop controller.

III. Consensus Control for NMG

Power sharing in low voltage MGs and poor power quality are challenging issues related to droop control, which are addressed in this section. Fig. 3 shows the control structure of droop controller as well as proposed consensus loops for improving droop controller performance in NMGs,

A. Power Sharing

To prevent DGs from overloading or even collapsing of MGs, the load demand must be dispersed among DG units proportionally to their available power capacity so that:

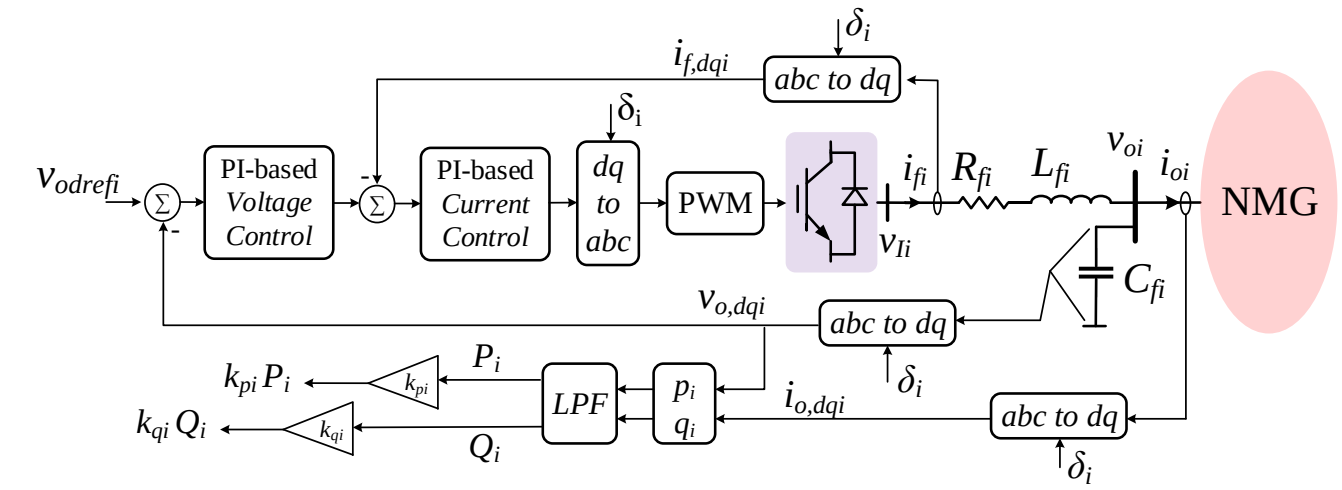

(a)

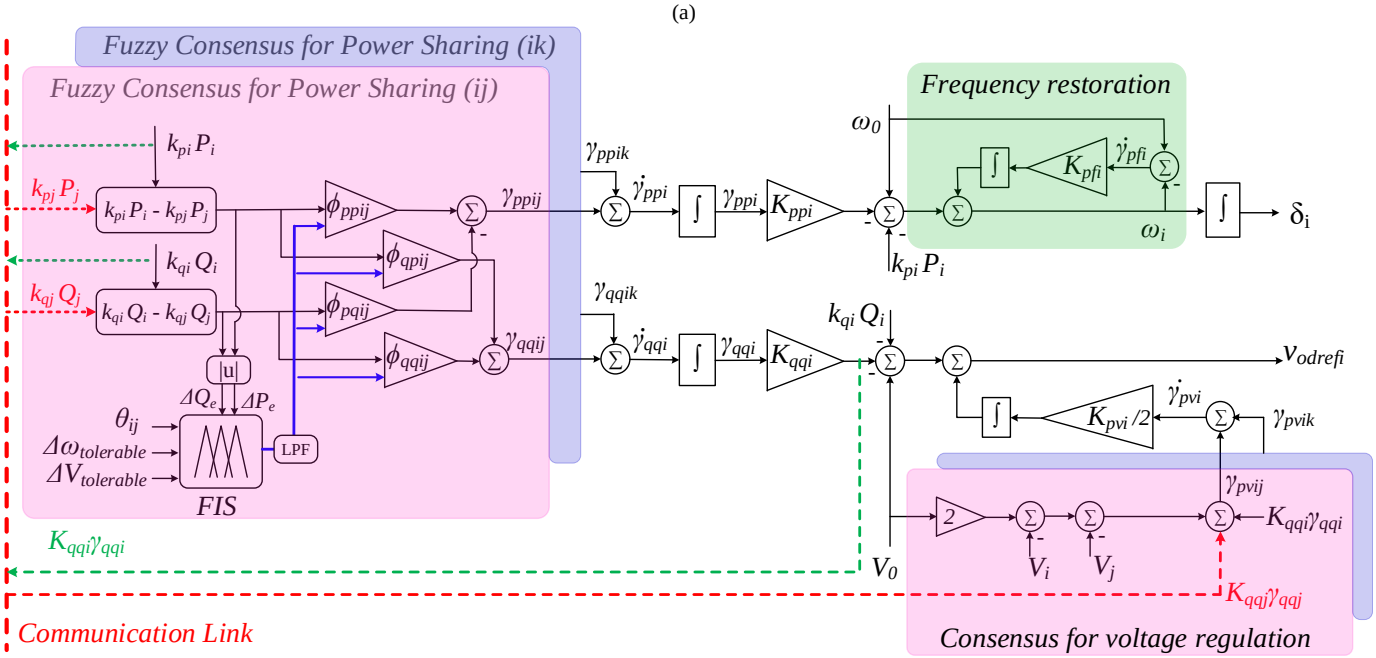

(b)

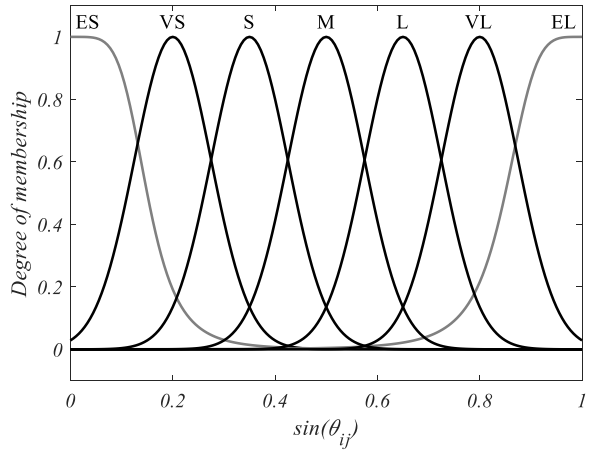

(c)

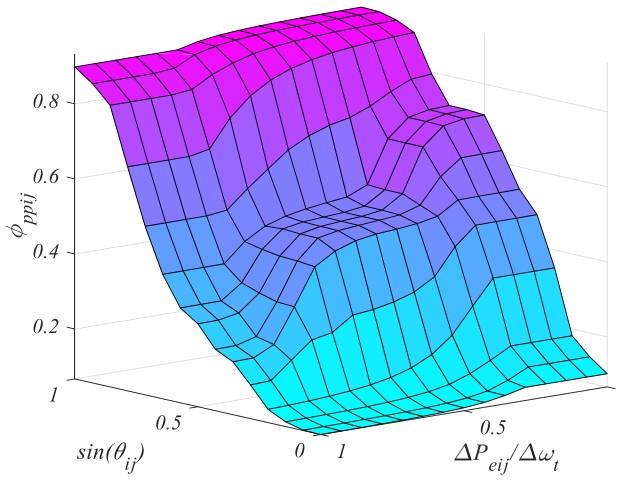

(d)

Fig. 3. The proosed control scheme: (a) VSI control system; (b) primary (droop) control loop and secondary control loop including fuzzy consensus as well as voltage regulation (consensus) and frequency restoration loops. In this figure, it is supposed that DG *i* is connected to DG *j* and DG *k* through power lines and communication links. Dashed lines denote communication links (red for receiving and green for sending data) and the communication link related to *ik*th loops is not shown for the sake of clarity. A low pass filter (LPF) is adopted after fuzzy interface system (FIS) to achieve a smoother fuzzy surface; (c) membership function for input 1; the ES and EL terms (refer to TABLE I for abbreviations) are represented by *gbellmf* and other terms are represented by *gaussmf*; (d) fuzzy surface for output 1 (ϕ_{ppij}) vs inputs 1 & 2.

TABLE I: FUZZY RULES

Input1	EL	VL	VL	VL	VL	L	L	L	L	M	M	M	S	S	S	S	VS	VS	VS	VS	ES
Input2	-	-	S	M	L	-	S	M	L	S	M	L	S	M	L	-	S	M	L	-	-
Input3	-	-	S	M	L	-	S	M	L	S	M	L	S	M	L	-	S	M	L	-	-
ϕ_{11}	EL	VL	EL	VL	M	L	EL	L	S	VL	M	VS	L	S	ES	S	M	VS	ES	VS	ES
ϕ_{12}	ES	VS	M	VS	ES	S	L	S	VS	L	M	S	VL	L	S	L	EL	VL	M	VL	EL
ϕ_{21}	ES	VS	M	VS	ES	S	L	S	VS	L	M	S	VL	L	S	L	EL	VL	M	VL	EL
ϕ_{22}	EL	VL	EL	VL	M	L	EL	L	S	VL	M	VS	L	S	ES	S	M	VS	ES	VS	ES

The abbreviation assigned to fuzzy terms are: Extremely Small (ES), Very Small (VL), Small (S), Medium (M), Large (L), Very Large (VL), and Extremely Large (EL). The "*if* … and *then* …" fuzzy rules are defined as: ***if*** input1=… & input2=… & input3=… ***then*** output1=… and so on.

$$k_{p1}P_1 = k_{pi}P_i \quad (\forall i = 2:n)\,(k_{pi} = \Delta\omega_{tolerable} / P_{nomi}) \tag{19}$$

$$k_{q1}Q_1 = k_{qi}Q_i \quad (\forall i = 2:n)\,(k_{qi} = \Delta V_{tolerable} / Q_{nomi}) \tag{20}$$

where $\Delta\omega_{tolerable}$ and $\Delta V_{tolerable}$ are permitted bands of angular frequency and voltage magnitude variation, P_{nomi} and Q_{nomi} are the nominal active and reactive power related to i^{th} DG unit.

Highlight 3: From the Jacobian matrices, *P* and *Q* variation related to the voltage magnitude and phase angle variations at bus *i* are given as in (21), assuming the *q* component is negligible:

$$\begin{bmatrix}\Delta P_{ij}\\ \Delta Q_{ij}\end{bmatrix} \approx \left[\begin{matrix}\frac{\partial P_{ij}}{\partial v_{odi}} & \frac{\partial P_{ij}}{\partial \delta_i}\\ \frac{\partial Q_{ij}}{\partial v_{odi}} & \frac{\partial Q_{ij}}{\partial \delta_i}\end{matrix}\right]_{\begin{bmatrix}\Delta v_{odi0}\\ \Delta\delta_{i0}\end{bmatrix}} \begin{bmatrix}\Delta v_{odi}\\ \Delta\delta_i\end{bmatrix} \tag{21}$$

$$\begin{bmatrix}\Delta P_{ij}\\ \Delta Q_{ij}\end{bmatrix} \approx \begin{bmatrix} 2\alpha_{ij}v_{odi0} - v_{odj0}\begin{pmatrix}+\alpha_{ij}cos(\delta_{ij0})\\ -\beta_{ij}sin(\delta_{ij0})\end{pmatrix} & v_{odi0}v_{odj0}\begin{pmatrix}+\alpha_{ij}sin(\delta_{ij0})\\ +\beta_{ij}cos(\delta_{ij0})\end{pmatrix}\\ 2\beta_{ij}v_{odi0} - v_{odj0}\begin{pmatrix}+\alpha_{ij}sin(\delta_{ij0})\\ +\beta_{ij}cos(\delta_{ij0})\end{pmatrix} & v_{odi0}v_{odj0}\begin{pmatrix}+\beta_{ij}sin(\delta_{ij0})\\ -\alpha_{ij}cos(\delta_{ij0})\end{pmatrix}\end{bmatrix}\begin{bmatrix}\Delta v_{odi0}\\ \Delta\delta_i\end{bmatrix}$$

where Δv_{odi0} and $\Delta\delta_{i0}$ are the values of Δv_{odi} and $\Delta\delta_i$ at a specific operating point, $\alpha_{ij}=sin(\theta_{ij})/Z_{ij}$ and $\beta_{ij}=cos(\theta_{ij})/Z_{ij}$. Noting that δ_{ij} is very small ($\delta_{ij}\approx 0$), from (21) we deduce:

if $X/R >> 1$: $\alpha\approx 0$ & $\beta\approx 1$ $\rightarrow$ $\Delta P \propto \Delta\delta$ & $\Delta Q \propto \Delta V$

if $X/R << 1$: $\alpha\approx 1$ & $\beta\approx 0$ $\rightarrow$ $\Delta P \propto \Delta V$ & $\Delta Q \propto -\Delta\delta$

However, the above Boolean logic is not applicable in MGs where the X/R ratio normally varies around one. So, the fuzzy coefficients may be adopted to model X/R ratio of interconnecting line impedances in the power sharing.

In order to tune fuzzy coefficients, more investigations are required. Assuming that X/R≈1, from (21) we have:

$$\begin{bmatrix}\Delta P_{ij}\\ \Delta Q_{ij}\end{bmatrix} \approx \frac{1}{Z_{ij}}\begin{bmatrix}|V| & |V|^2\\ |V| & -|V|^2\end{bmatrix}\begin{bmatrix}\Delta v_{odi}\\ \Delta\delta_i\end{bmatrix} \tag{22}$$

Two important conclusive observations can be obtained from (22): 1) the sensitivity of ΔP and ΔQ to the voltage magnitude is proportional to the voltage magnitude, while their sensitivity to the phase angle is proportional to the square of voltage magnitude; 2) active power sharing is in conflict with reactive power sharing in NMGs with low X/R ratio of grid impedance, since $\Delta\delta$ causes opposite effects on *P* and *Q* control. The problem comes from the fact that as $\Delta\delta$ is adopted for active power sharing in conventional droop controllers, while it makes reactive power sharing far worse (reactive power sharing is not implemented accurately by conventional *V-Q* droop control because of the voltage drop over power lines). Even though a supplementary control strategy has been employed for accurate *Q* sharing, more control efforts would be required, which leads to more voltage deviation. So, in order to reach the precise active and reactive power sharing, the droop control (6)-(7) is modified as:

$$\dot{\delta}_i = -k_{pi}P_i - K_{ppi}\gamma_{ppi} \tag{23}$$

$$V_{refi} = V_0 - k_{qi}Q_i - K_{qqi}\gamma_{qqi} \tag{24}$$

where γ_{pp} and γ_{qq} are consensus control signals, and K_{pp} and K_{qq} are consensus gains. According to the explanation, which is given earlier from (21)-(22), the fuzzy-based consensus signals are defined as:

$$\dot{\gamma}_{ppi} = \sum_{j=1}^{n}\phi_{ppij}\,\sigma_{ij}\,(k_{pi}P_i - k_{pj}P_j) - \sum_{j=1}^{n}\phi_{pqij}\,\sigma_{ij}\,(k_{qi}Q_i - k_{qj}Q_j) \tag{25}$$

$$\dot{\gamma}_{qqi} = \sum_{j=1}^{n}\phi_{qpij}\,\sigma_{ij}\,(k_{pi}P_i - k_{pj}P_j) + \sum_{j=1}^{n}\phi_{qqij}\,\sigma_{ij}\,(k_{qi}Q_i - k_{qj}Q_j) \tag{26}$$

where ϕ_{ppij}, ϕ_{pqij}, ϕ_{qpij}, ϕ_{qqij} are fuzzy coefficients tuned dynamically by a fuzzy controller presented as follows:

Fuzzy interface system (FIS)*:* the Mamdani's FIS [31], which is the most common fuzzy controller, is adopted and consists of the following parts:

1) Inputs: inputs to the FIS are given as follows:

$$\begin{cases} Input\,1 = \sin(\theta_{ij}) \\ Input\,2 = \left|k_{pi}P_i - k_{pj}P_j\right| / \Delta\omega_{tolerable} \coloneqq \Delta P_e / \Delta\omega_t \\ Input\,3 = \left|k_{qi}Q_i - k_{qj}Q_j\right| / \Delta V_{tolerable} \coloneqq \Delta Q_e / \Delta V_t \end{cases}$$

The first input is *sin* (θ_{ij}) which represents a unified factor of X/R ratio of the impedance of the ij^{th} power line. The second and third inputs are the amount of inaccuracy of active and reactive power sharing, in a per-unit form.

2) Fuzzification by applying fuzzy memberships to the inputs. To this end, the Gaussian curve membership function (*gaussmf*) is adopted to achieve smoothness and concise notation. The generalized bell-shaped membership function (*gbellmf*) is also used in the FIS. The *gbellmf* has more flexibility than *gaussmf* to approach non-fuzzy values, e.g. values of input 1, which are closed to 0 or 1. The membership function plot for the first input is depicted in Fig. 3(c).

3) Fuzzy rules reflect fuzzified inputs to the fuzzified outputs. Two control objectives are followed when designing fuzzy rules:

- In order to take the X/R ratio of the power lines into account according to *Highlight 3* and based on (21).
- In order to achieve smooth transient and to improve the dynamic stability margins. To this end, the larger inaccuracy

of power sharing the smaller control gains. By adopting this rule, the control gains are small just after a disturbance and become larger as the system approaches to steady state to provide a virtual inertia to the input control signals. This is particularly important for NMG in which the interaction of droop controllers is high (*Highlight 1*). The designed fuzzy rules are given in Table I.

4) Fuzzified outputs (ϕ_{ppij}, ϕ_{pqij}, ϕ_{qpij}, ϕ_{qqij}) are determined by mapping the fuzzified inputs to output membership functions through fuzzy rules. Here the triangular membership function (*trimf*) is adopted for the outputs of the fuzzy interface system.

5) Defuzzification of fuzzified outputs (ϕ_{ppij}, ϕ_{pqij}, ϕ_{qpij}, ϕ_{qqij}) to the permitted band determined based on sensitivity of ΔP & ΔQ to ΔV & $\Delta\delta$ given from (21)-(22).

The advantage of the proposed fuzzy controller over virtual impedance [14], [19], [32] is as follows. Although virtual impedance decouples *f-P* and *V-Q* droop loops to some extent, the reactive power sharing is still an issue or even worse due to non-uniform voltage drops at generation nodes. The voltage drop due to virtual impedance also leads to poor power quality and also limits the maximum transferable power [32]. Furthermore, in the conventional *V-Q* droop loop v_{oq} is considered zero. It is a general agreement to fix the initial point of all converters to a reference point for the synchronization and power sharing purposes. It is also useful to regulate the voltage magnitude and coordinate droop controllers with only one variable (v_{od}). However, v_{oq} would not be zero with the virtual impedance method. On the other hand, precise active and reactive power sharing are achieved through the proposed fuzzy consensus protocol, without imposing the disadvantages of virtual impedance to the system. Moreover, stability of the proposed fuzzy control system is guaranteed by adopting the output feedback stabilization method which is presented in Section III-C.

B. Power Quality

Droop control operation in power sharing leads to the deviation of power system variables from their nominal values and thus poor power quality. Concerning the frequency restoration and voltage regulation, the reference voltage and phase angle at each generation bus in (23)-(24) are further modified as:

$$\dot{\delta}_i = -k_{pi} P_i - K_{ppi}\gamma_{ppi} - K_{pfi}\gamma_{pfi} \tag{27}$$

$$V_{i,ref} = V_0 - k_{qi} Q_i - K_{qqi}\gamma_{qqi} - K_{qvi}\gamma_{qvi} \tag{28}$$

where γ_{pf} and γ_{qv} are consensus control signals given in (29)-(30), respectively, K_{pf} and $K_{qv,}$ are the consensus gains for restoring voltage and frequency to the nominal values.

$$\dot{\gamma}_{pfi} = \left(\omega_i - \omega_0\right) \tag{29}$$

$$\dot{\gamma}_{qvi} = \sum_{j=1}^{n}\sigma_{ij}\left(\frac{\left(V_i + V_j\right) - \left(K_{qqi}\gamma_{qqi} + K_{qqj}\gamma_{qqj}\right)}{2} - V_0\right) \tag{30}$$

It is worth noting that the integral term of ω-ω_0 in (29) may cause the active power sharing to be inaccurate, since it imposes an offset to the phase angle [33]. However, it is recovered by the consensus signals given in (25)-(26) properly.

Highlight 4: As voltage is not a global variable throughout the NMG due to voltage drop over the power lines impedance, the voltages at NMG nodes cannot be regulated strictly to a constant value (the nominal voltage). Besides, by restoring the voltage magnitude at NMG nodes to a fixed value, the *Q*-sharing accuracy will be lost. However, the voltage profile across the NMG must be maintained within a permitted band. In other words, the voltage magnitude at power network nodes can be a varying, according to reactive power sharing purpose, but within a tolerable band. To this end, the average voltage profile, which is dropped because of the droop control effect (V_0-k_qQ), is compensated by (30), while still keeping the reactive power sharing accurate. For a better sense of (30) please see the voltage magnitude axis in Fig. 4. After reaching the accurate reactive power sharing by the consensus signal, the voltage references at all DG unit controllers, V_{refi}, consist of two parts: 1) droop control signals, $V_{ref,droopi} = V_0 - k_{qi}Q_i$, which are equal at all DG units according to (20), denoted by $V_{ref,droop}$; and 2) consensus signals, $V_{ref,consensusi} = K_{qqi}\gamma_{qqi}$ which cause the voltage magnitudes, V_{refi} and $V_{refj,}$ shift up or down depending on the consensus signals signs and consensus gains amplitude (before restoration). So, the consensus protocol (30) removes the droop control offset, and raises the voltage profile to the nominal band (after restoration); at the same time, the power sharing is implemented accurately, provided that the consensus time constant is larger than those of the droop controller and fuzzy consensus in (23)-(24).

C. Consensus gains determination as structured static output feedback stabilization problem

Consensus control adds four more states per DG unit to the small signal model of NMG. Having a closer view to the consensus signals reveals that the proposed consensus control is a kind of output feedback control, and consensus gains might be considered as output feedback gains. In the state space design, output feedback gains are determined so that the closed loop poles are located in the desired place. To this end, considering consensus signals as outputs of the system, we are dealing with a reduced-order static output feedback stabilization problem. For the given consensus-based NMG system, neglecting the load disturbances ($\Delta i_{L,dqi}$), the augmented state space model is obtained as:

$$\dot{x}_c = A_c x_c + B_c u_c \qquad y_c = C_c x_c \tag{31}$$

where the subscript "*c*" denotes the consensus-based NMG model which is obtained by inserting (25)-(26) and (29)-(30) into the NMG model (18);

$$x_c = \left[x_{c1},\ldots,x_{cn}\right]^T,\ x_{ci} = \left[x_i, \gamma_{ppi}, \gamma_{pfi}, \gamma_{qqi}, \gamma_{qvi}\right]^T$$

$$u_c = \left[u_{c1},\ldots,u_{cn}\right]^T,\quad u_{ci} = \begin{bmatrix} K_{ppi}\gamma_{ppi} + K_{pfi}\gamma_{pfi} \\ K_{qqi}\gamma_{qqi} + K_{qvi}\gamma_{qvi} \\ -\sum_{j=1}^{n}\sigma_{ij}\left(K_{qqj}\gamma_{qqj} + K_{qqi}\gamma_{qqi}\right) \end{bmatrix}$$

$$y_c = \left[y_{c1},\ldots,y_{cn}\right]^T,\ y_{ci} = \left[\gamma_{ppi}, \gamma_{pfi}, \gamma_{qqi}, \gamma_{qvi}\right]^T$$

$$A_c \in R^{(15n)\times(15n)},\ B_c \in R^{(15n)\times(3n)},\ C_c \in R^{(4n)\times(15n)}$$

$$B_c = diag\left[B_{c1}...B_{ci}...B_{cn}\right]$$

$$B_{ci} = \begin{bmatrix} -1 & 0 & 0 & 0 & 0 & 0 & 0 & 0 & 0_{6\times1} & 0 \\ 0 & 0 & 0 & -1 & 0 & -k_{pv} & 0 & -k_{pv}k_{pc}/L_f & 0_{6\times1} & 0 \\ 0 & 0 & 0 & 0 & 0 & 0 & 0 & 0 & 0_{6\times1} & -1 \end{bmatrix}^T$$

$$C_c = diag\left[C_{c1},\ldots,C_{cn}\right], C_{ci} = \left[0_{4\times7} \quad I_4\right]$$

where I_4 is the identity matrix of dimension 4. The output consensus signals are inserted to the control system as inputs:

$$u_c = K_c\, y_c = K_c\, C_c\, x_c \tag{32}$$

where $K_c \in R^{(3n)\times(4n)}$ has the following inheriting structure:

$$K_c = \left[K_{cij}\right]_{n\times n}$$

$$K_{cii} = \begin{bmatrix} K_{ppi} & K_{pfi} & 0 & 0 \\ 0 & 0 & K_{qqi} & K_{qvi} \\ 0 & 0 & -\sum_j^n \sigma_{ij} K_{qqi} & 0 \end{bmatrix}, K_{cij} = \begin{bmatrix} 0 & 0 & 0 & 0 \\ 0 & 0 & 0 & 0 \\ 0 & 0 & -\sigma_{ij} K_{qqj} & 0 \end{bmatrix} \tag{33}$$

Accordingly, the updated state matrix is obtained as:

$$\dot{x}_c = \left(A_c + B_c\, K_c\, C_c\right) x_c \tag{34}$$

Various methods have been proposed to find the static output feedback gain matrix (K_c) [34]-[36]. Based on the LMI technique [36], the full static output feedback matrix exists if and only if there exist matrices X and S and scalar $\lambda > 0$ so that:

$$\begin{aligned} &B_{c\perp}\left(A_c\, X + X\, A_c^T + 2\lambda\, X\right) B_{c\perp}^T \le 0 \\ &C_{c\perp}^T\left(A_c^T\, S + S\, A + 2\lambda\, S\right) C_{c\perp} \le 0 \\ &\kappa\left(X, S\right) = \begin{bmatrix} X & I \\ I & S \end{bmatrix} \ge 0 \end{aligned} \tag{35}$$

and *Rank* $\kappa(X,S) \le 15n$, where $C_c\perp$ denotes the matrix with maximal rank such that $C_c C_c\perp = 0$, and $B_c\perp$ denotes the matrix with maximal rank such that $B_c\perp B_c = 0$. This ensures real parts of the closed loop eigenvalues are less than or equal to $-\lambda$. The cone complementarity linearization algorithm [36] is used to minimize the bilinear objective (36) under LMI constraints (35) to find the matrices X and S.

$$min\ Trace\ (X\ S)\ \ subject\ to\ (35) \tag{36}$$

Finally, the structured static output feedback gain matrix K_c is obtained by solving the following LMI subject to the structure constraint (33):

$$\left(A_c + B_c\, K_c\, C_c\right) X + X\left(A_c + B_c\, K_c\, C_c\right)^T + 2\lambda X \le 0 \tag{37}$$

IV. Simulation Results and Eigen-Analysis

The NMG, depicted in Fig. 5, is simulated in MATLAB\ Simulink to evaluate the effectiveness of the proposed method.

A. Model Validation

Critical dominant modes: Critical dominant modes of the droop-controlled NMG are depicted in Fig. 6(a). Those with low frequency oscillations and large time constant are associated with *f-P* droop loop.

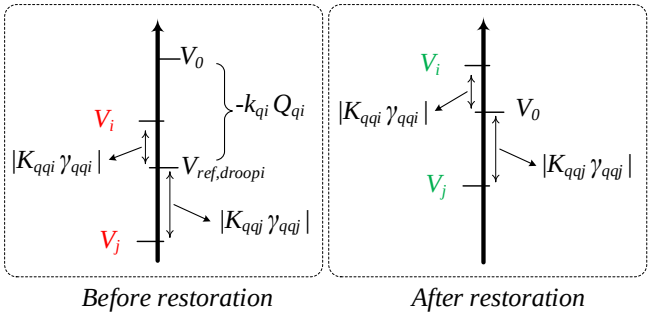

Fig. 4. The consensus algorithm for average voltage profile restoration.

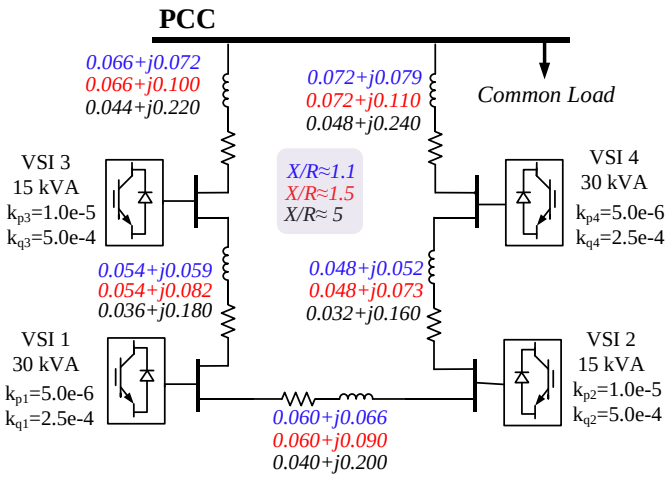

Fig. 5. Simulated NMG with four voltage source inverters (VSIs): the blue colour is related to the power network with X/R=1.1; the red colour is related to the power network topology with X/R=1.5; the black colour is related to the power network topology with X/R=5. Additional control parameters related to the VSI's inner control loops and LC filter are presented in Appendix B.

On the other hand, those indicating high frequency fluctuations with small time constant are related to *V-Q* control loop including droop controller, VSI inner loops and LC filter. Moreover, the eigenvalue of the NMG with different X/R ratios are compared as well. The NMG with X/R=1.1 is unstable which is proved with both eigenvalue loci and time domain results in Figs. 6(a), (b), while X/R=1.5 makes the control system stable, as shown in Figs. 6(a) and (c).

Critical dominant modes and cross-coupling effect: The dominant eigenvalue loci of the conventional *f-P* and *V-Q* droop loops are shown in Figs. 7(a) and (b) for different X/R ratios (1.5 and 5). It is observed that increasing the corresponding droop gains (arrow direction) shifts the related eigenvalues toward the right half s-plane (the unstable region). The following observations can be concluded from the root loci:

i. The cross-coupling effect is represented by the eigenvalue loci well; as it is expected, the higher X/R ratio the lower cross coupling effect. It is evident in Fig. 7(b) that the variation of *f-P* droop gains has less effect on the critical eigenvalues related to the *V-Q* droop loop, and vice versa, compared to Fig. 7(a).

ii. Increasing the droop gain of a given loop has an opposite effect on the other loop as concluded earlier from (22). It can be seen that increasing the droop gains of *f-P* droop loops, while shifting relevant eigenvalues to the right side in s-

plane, shifts the critical models of *V-Q* droop loop toward the left side and vice versa.

iii. The stability margin is improved with increased X/R ratio since less eigenvalues are located in the unstable region in Fig. 7(b) compared to Fig. 7(a).

iv. With the higher X/R ratio, the oscillation mode with lower frequency (closer to the center) is related to *f-P* droop loop, while the higher frequency oscillation is related to *V-Q* droop loop.

v. The lower X/R ratio, the closer oscillation frequency of *f-P* and *V-Q* loops since the relevant eigenvalues to *V-Q* droop loops are getting closer to those related to *f-P* droop loop.

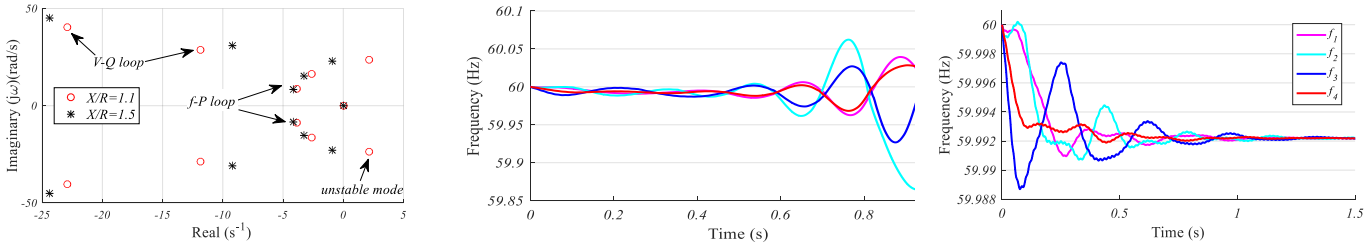

(a) (b) (c)

Fig. 6. Eigenvalue analysis and simulation results: (a) critical dominant modes for MG with different X/R ratios (1.1 and 1.5); (b) frequency dynamic of MG with X/R=1.1, which is unstable; (c) frequency dynamic of MG with X/R=1.5, which is stable.

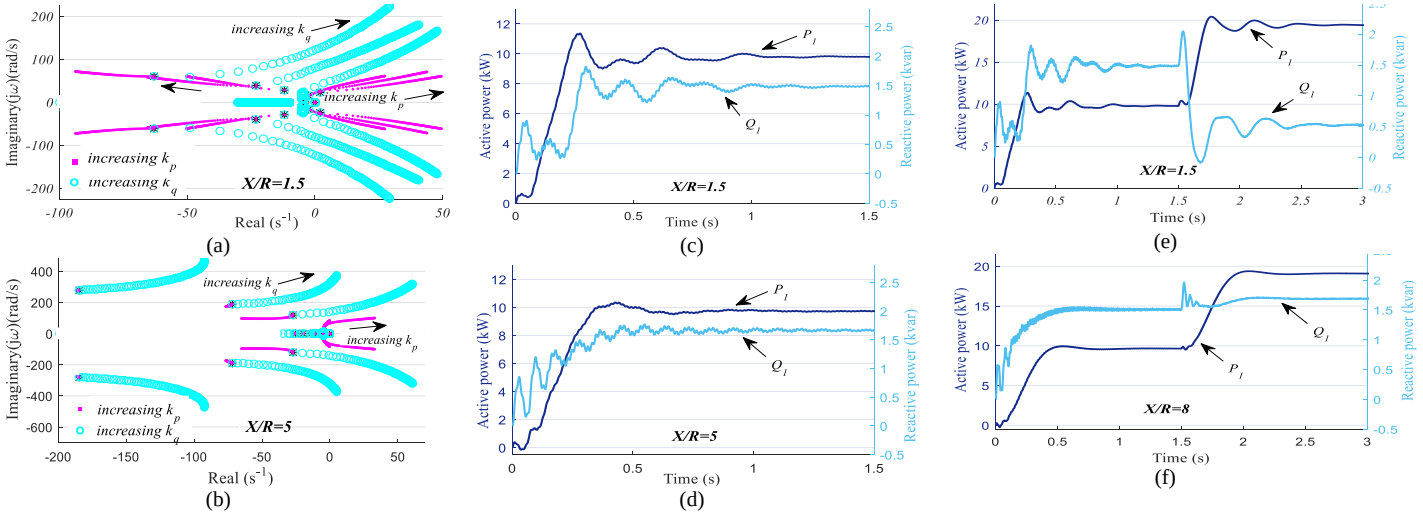

(a) (b) (c) (d) (e) (f)

Fig. 7. Dominant oscillation modes: (a), (b) eigenvalue loci of *f-P* and *V-Q* droop loops; (c), (d) active and reactive power oscillations; (e), (f) *P* and *Q* coupling (active load is changed while reactive load is constant).

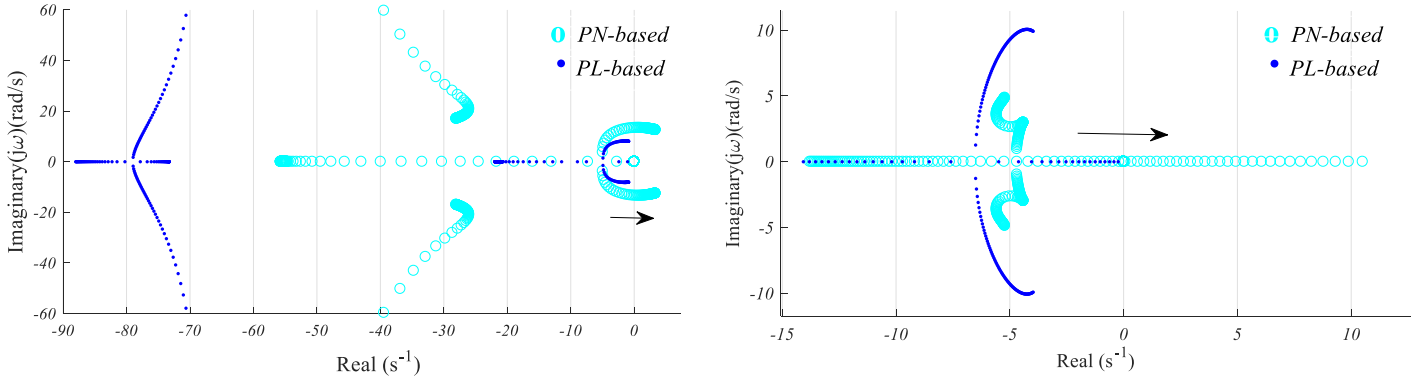

(a) (b)

Fig. 8. Dominant eigenvalue comparison between power network-based (PN-based) model and parallel-based (PL-based) model: (a) decreasing (arrow direction) inductance of the grid impedance (0.1 < X/R < 10); (b) increasing $\Delta\delta_{ij}$ (arrow direction).

Simulation results are provided in Figs. 7(c) and (d) to validate the above-mentioned observations given from the proposed model. Fig. 7(c) shows that with X/R ratio around 1.5, the *f-P* and *V-Q* droop loops are tightly coupled as both oscillate roughly with the same frequency. Fig. 7(d) reveals that with X/R ratio around five, the control loops are less coupled, as the frequency of *f-P* mode is lower than that related to *V-Q* droop loops. Nevertheless, the high oscillation mode related to the *V-Q* droop loop is modulated on the output active power and vice versa. Figs. 7 (e) and (f) compare time domain simulation results for X/R ratio of 1.5 and 8, respectively, in which the active load is changed at *t*=1.5 seconds while the reactive load is kept constant. With X/R ratio of 1.5, *P* variation leads to dramatic inverse *Q* variation as both *P* and *Q* control loops are

strongly coupled. With X/R ratio of 8, the *V-Q* control loop is decoupled from *f-P* (phase angle) control loop and only affected by the voltage drop through the power network impedance.

Comparison: A comparison between the eigenvalue loci of the developed power network-based (PN-based) model and conventional parallel-based (PL-based) model [26] is presented in Fig. 8. The developed model reveals the stability boundaries of the control system in relation to grid impedance parameters (decreasing X/R ratio of the power lines), and phase angle difference at NMG buses, as a consequence of load increase. While, the parallel-based model does not reveal the unstable regions accurately.

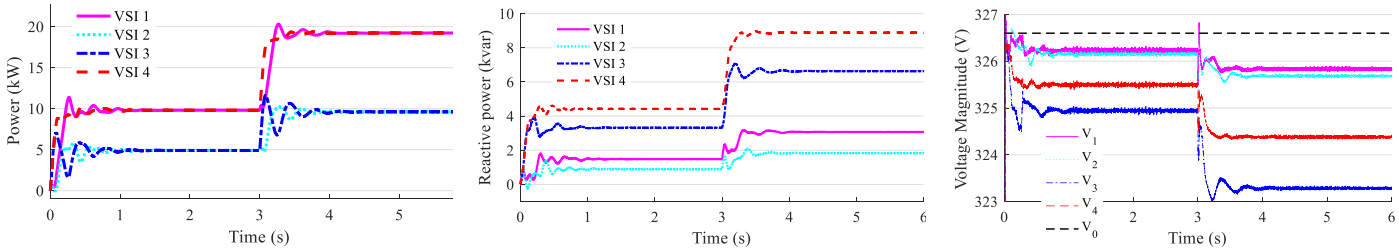

Fig. 9. Simulation results for conventional droop control: (a) active power sharing; (b) reactive power sharing; (c) voltage magnitude.

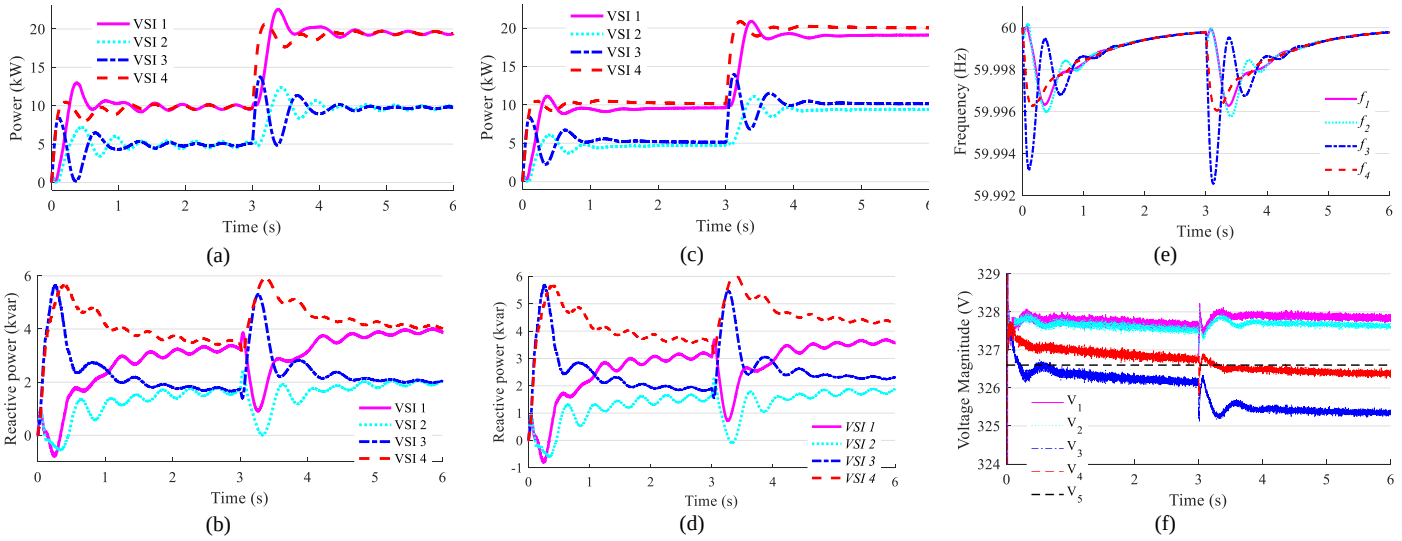

Fig. 10. Simulation results for conventional consensus control: (a), (b) active and reactive power sharing without frequency and voltage restoration loops; (c), (d) active and reactive power sharing with frequency and voltage restoration loops; (e) frequency restoration; (f) voltage restoration.

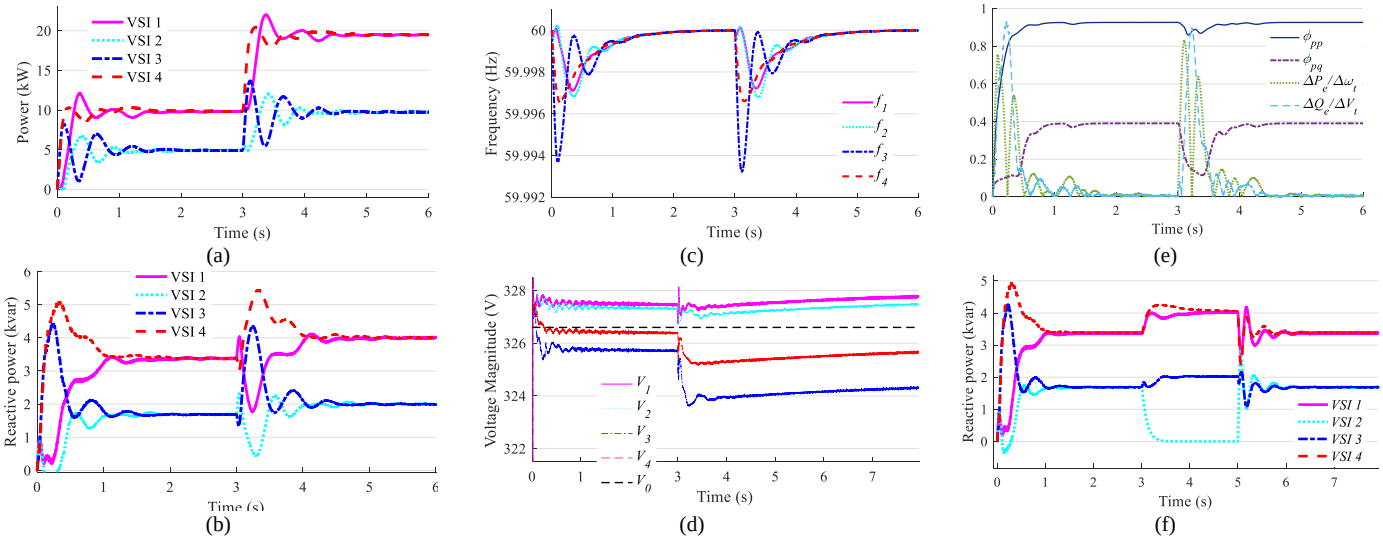

Fig. 11. Simulation results for the proposed method: (a), (b) active and reactive power sharing through the proposed fuzzy consensus protocol; (c), (d) frequency and voltage restoration; (e) fuzzy gains; (f) Q-sharing by proposed method, VSI 2 is switched off at t = 3 s and switched on at t = 5 s.

A. Consensus control performance

For the time domain study in this section, the NMG with X/R=1.5 is adopted for the Simulink model. The effective fuzzy coefficients are determined through multiplying the FIS outputs by their corresponding maximum (nominal) values given in Table II. The consensus gains are determined by solving the LMI-based structured static output feedback stabilization problem. YALMIP [37], a MATLAB toolbox for rapid prototyping optimization problems is used to obtain the optimal feedback gains along with modified droop gains, which are presented in Table II. Since accurate active and reactive power sharing are established through adopting the proposed fuzzy consensus protocols, smaller droop gains are adopted to improve dynamic performance and stability margins.

Table II. Control parameters adopted for simulations.

Fuzzy parameters	$\phi_{ppij,max}$	$\phi_{pqij,max}$	$\phi_{qpij,max}$	$\phi_{qqij,max}$
	1	0.0375	50	1
Consensus gains	K_{pp}	K_{qq}	K_{pf}	K_{qv}
	1.15	2.3	1.6	0.025
***f-P* droop gains**	k_{p1}	k_{p2}	k_{p3}	k_{p4}
	2.5e-6	5e-6	5e-6	2.5e-6
***V-Q* droop gains**	k_{q1}	k_{q2}	k_{q3}	k_{q4}
	1e-4	2e-4	2e-4	1e-4

In this case study, a common load (P=30 kW and Q=10 kVAr) is connected to the autonomous MG at t=0 (s). Then the same load is added at t=3 (s) to analyze the system dynamics when a load change happens as a disturbance.

Droop control performance: The performances of the conventional *f-P* and *V-Q* droop controllers are illustrated in Fig. 9. Although the active power sharing is implemented accurately, as shown in Fig. 9(a), accurate reactive power sharing is not achieved, as shown in Fig. 9(b). In order to achieve a precise reactive power sharing, the output reactive power of DG units should be proportional to their droop gains, i.e. the output reactive power of VSIs 1 & 4 should be same and twice as those of VSIs 2 & 3, since the droop gains of the former ones are half of the droop gains of the latter ones. Besides, the frequency and voltage magnitude deviate from the nominal values as a consequence of droop rules, as shown in Fig. 6(c) and Fig. 9(c), which are the major drawbacks of the droop control system.

Conventional consensus control: The performance of the conventional consensus protocols presented in [20]-[21] is evaluated in Fig. 10, when the X/R ratio is low (X/R=1.5). First, the performance of the consensus protocol for active and reactive power sharing is considered without taking the voltage and frequency restoration loops into account, which is illustrated in Figs. 10(a) & (b). The system is oscillatory and Q-sharing is not achieved with a desirable dynamic response. The situation becomes worse when the voltage and frequency restoration loops are taken into account. There is an error in the active power sharing, which becomes larger after each disturbance, as shown in Fig. 10(c), and the reactive power sharing is almost lost.

Proposed fuzzy consensus protocols as well as proposed frequency and voltage restoration loops: The performance of the proposed fuzzy consensus protocol for active and reactive power sharing is indicated in Figs. 11(a) & (b), which reveal a significant improvement in dynamic performance, compared to Figs. 10(a) & (b), thanks to the fuzzy consensus protocol by which the X/R ratio of the power lines is taken into account. Despite of the networked topology of the NMG, and low X/R ratio (X/R ≈1.5), the active and reactive power sharing is implemented well according to the assigned droop gains. Along with the fuzzy consensus for power sharing, the proposed voltage and frequency restoration loops are adopted. As it is demonstrated in Figs. 11(c) the frequency is restored to the nominal value while precise active power sharing is preserved. In addition, the power quality is improved by raising the voltage profile to the nominal band, as shown in Fig. 11(d), while, it is not conflicted with the reactive power sharing. On the other hand, the permitted voltage band, i.e. the minimum and maximum acceptable value for voltage at NMG nodes, must be respected not to be violated. However, this issue falls in the MG design process when the power network topology and sizing, allocation and sizing of DG units, loads and VAr compensators, and so on are taken into account, which is beyond the scope of this work. The fuzzy coefficients related to the power sharing protocol are given in Fig. 11(e). The VSI 2 is switched off and on at t = 3 s and t = 5 s, respectively, as shown in Fig. 11(f). After disconnection of VSI 2, the reactive power is supported by other VSIs, proportional to their droop gains. The system returns to its initial condition when VSI 2 is reconnected, and the system is stabilized.

V. CONCLUSION

It was found that the interaction of droop controllers is high in NMGs with loose power networks due to the low X/R ratio and lack of inertia in the inverter's control system, which narrows the stability margins. Also, inadequacy of the conventional parallel-based small-signal model for autonomous MGs was explored. Therefore, a novel small signal model for NMGs was developed where the interaction of droop controllers through the power network is realized. The eigenvalue analysis revealed the cross-coupling effect between *f-P* and *V-Q* droop loops as well as unstable regions considering X/R ratio of the power lines. In addition, two new consensus protocols were defined for power sharing and power quality improvement. Power sharing is implemented well regardless of the grid impedance nature by tuning some fuzzy coefficients representing the X/R ratio of the interconnecting power lines. Also dynamic performance of the system is significantly improved via the proposed fuzzy controller. Furthermore, power quality is improved by raising the average voltage profile at NMG buses also in accordance with reactive power sharing. This is achieved by proposing a consensus algorithm, which removes the droop control offset and moves the average voltage profile to the permitted band. Finally, the consensus gains were designed by employing a structured static output feedback stabilization problem. It was solved by an LMI method, guaranteeing stability of the closed-loop NMG system. The time domain study through the simulations revealed considerable improvement of the proposed method compared to the conventional consensus protocols.

APPENDIX A
JACOBIAN MATRICES

$$J_{ii}=\begin{bmatrix}
0 & -k_{pi} & 0 & 0 & 0 & 0 & 0 & 0 & 0 & 0 & 0\\
\omega_c\sum_{j=1}^{n}\sigma_{ij}\frac{\partial P_{ij}}{\partial \delta_i} & -\omega_c & 0 & 0 & 0 & 0 & 0 & 0 & 0 & \omega_c\left(i_{Ldi0}+\sum_{j=1}^{n}\sigma_{ij}\frac{\partial P_{ij}}{\partial v_{odi}}\right) & \omega_c\left(i_{Lqi0}+\sum_{j=1}^{n}\sigma_{ij}\frac{\partial P_{ij}}{\partial v_{oqi}}\right)\\
\omega_c\sum_{j=1}^{n}\sigma_{ij}\frac{\partial Q_{ij}}{\partial \delta_i} & 0 & -\omega_c & 0 & 0 & 0 & 0 & 0 & 0 & \omega_c\left(-i_{Lqi0}+\sum_{j=1}^{n}\sigma_{ij}\frac{\partial Q_{ij}}{\partial v_{odi}}\right) & \omega_c\left(i_{Ldi0}+\sum_{j=1}^{n}\sigma_{ij}\frac{\partial Q_{ij}}{\partial v_{oqi}}\right)\\
0 & 0 & -k_{qi} & 0 & 0 & 0 & 0 & 0 & 0 & -1 & 0\\
0 & 0 & 0 & 0 & 0 & 0 & 0 & 0 & 0 & 0 & -1\\
F_i & 0 & -k_{pvi}\,k_{qi} & k_{Ivi} & 0 & 0 & 0 & -1 & 0 & -k_{Pvi}+F_i & -\omega_0 C_{fi}+F_i\\
F_i & 0 & 0 & 0 & k_{Ivi} & 0 & 0 & 0 & -1 & \omega_0 C_{fi}+F_i & -k_{Pvi}+F_i\\
\left(\frac{F_i k_{Pci}}{L_{fi}}\sum_{j=1}^{n}\sigma_{ij}\frac{\partial i_{dij}}{\partial \delta_i}\right) & -k_{pi}\,i_{fqi0} & \frac{-k_{Pci}\,k_{Pvi}\,k_{qi}}{L_{fi}} & \frac{k_{Pci}k_{Ivi}}{L_{fi}} & 0 & \frac{k_{Ici}}{L_{fi}} & 0 & \frac{-R_{fi}-k_{pci}}{L_{fi}} & -k_{pi}P_{0i} & \left(\frac{1-k_{Pvi}\,k_{Pci}}{L_f}+\frac{F_i\,k_{Pci}}{L_{fi}}\sum_{j=1}^{n}\sigma_{ij}\frac{\partial i_{dij}}{\partial v_{odi}}\right) & \left(-\frac{\omega_0 C_{fi}\,k_{Pci}}{L_{fi}}+\frac{F_i k_{Pci}}{L_{fi}}\sum_{j=1}^{n}\sigma_{ij}\frac{\partial i_{dij}}{\partial v_{oqi}}\right)\\
\left(\frac{F_i k_{Pci}}{L_{fi}}\sum_{j=1}^{n}\sigma_{ij}\frac{\partial i_{qij}}{\partial \delta_i}\right) & k_{pi}i_{fdi0} & 0 & 0 & \frac{k_{Pci}k_{Ivi}}{L_{fi}} & 0 & \frac{k_{Ici}}{L_{fi}} & k_{pi}P_{0i} & \frac{-R_{fi}-k_{Pci}}{L_{fi}} & \left(\frac{\omega_0 C_{fi}\,k_{Pci}}{L_{fi}}+\frac{F_i\,k_{Pci}}{L_{fi}}\sum_{j=1}^{n}\sigma_{ij}\frac{\partial i_{qij}}{\partial v_{odi}}\right) & \left(\frac{1-k_{Pvi}\,k_{Pci}}{L_f}+\frac{F_i k_{Pci}}{L_{fi}}\sum_{j=1}^{n}\sigma_{ij}\frac{\partial i_{qij}}{\partial v_{oqi}}\right)\\
\frac{-1}{C_{fi}}\sum_{j=1}^{n}\sigma_{ij}\frac{\partial i_{dij}}{\partial \delta_i} & -k_{pi}v_{oqi0} & 0 & 0 & 0 & 0 & 0 & \frac{1}{C_{fi}} & 0 & \frac{-1}{C_{fi}}\sum_{j=1}^{n}\sigma_{ij}\frac{\partial i_{dij}}{\partial v_{odi}} & \left(\omega_0-k_{pi}P_{0i}+\frac{-1}{C_{fi}}\sum_{j=1}^{n}\sigma_{ij}\frac{\partial i_{dij}}{\partial v_{oqi}}\right)\\
\frac{-1}{C_{fi}}\sum_{j=1}^{n}\sigma_{ij}\frac{\partial i_{qij}}{\partial \delta_i} & k_{pi}v_{odi0} & 0 & 0 & 0 & 0 & 0 & 0 & \frac{1}{C_{fi}} & \left(\omega_0-k_{pi}P_{0i}+\frac{-1}{C_{fi}}\sum_{j=1}^{n}\sigma_{ij}\frac{\partial i_{qij}}{\partial v_{odi}}\right) & \frac{-1}{C_{fi}}\sum_{j=1}^{n}\sigma_{ij}\frac{\partial i_{qij}}{\partial v_{oqi}}
\end{bmatrix}$$

$$J_{ij}=\begin{bmatrix}
0 & 0 & 0 & 0 & 0 & 0 & 0 & 0 & 0 & 0 & 0\\
\omega_c\frac{\partial P_{ij}}{\partial \delta_j} & 0 & 0 & 0 & 0 & 0 & 0 & 0 & 0 & \omega_c\frac{\partial P_{ij}}{\partial v_{odj}} & \omega_c\frac{\partial P_{ij}}{\partial v_{oqj}}\\
\omega_c\frac{\partial Q_{ij}}{\partial \delta_j} & 0 & 0 & 0 & 0 & 0 & 0 & 0 & 0 & \omega_c\frac{\partial Q_{ij}}{\partial v_{odj}} & \omega_c\frac{\partial Q_{ij}}{\partial v_{oqj}}\\
0 & 0 & 0 & 0 & 0 & 0 & 0 & 0 & 0 & 0 & 0\\
0 & 0 & 0 & 0 & 0 & 0 & 0 & 0 & 0 & 0 & 0\\
F_i & 0 & 0 & 0 & 0 & 0 & 0 & 0 & 0 & F_i & F_i\\
F_i & 0 & 0 & 0 & 0 & 0 & 0 & 0 & 0 & F_i & F_i\\
\left(\frac{F_i k_{Pci}}{L_{fi}}\frac{\partial i_{dij}}{\partial \delta_j}\right) & 0 & 0 & 0 & 0 & 0 & 0 & 0 & 0 & \left(\frac{F_i k_{Pci}}{L_{fi}}\frac{\partial i_{dij}}{\partial v_{odj}}\right) & \left(\frac{F_i k_{Pci}}{L_{fi}}\frac{\partial i_{dij}}{\partial v_{oqj}}\right)\\
\left(\frac{F_i k_{Pci}}{L_{fi}}\frac{\partial i_{qij}}{\partial \delta_j}\right) & 0 & 0 & 0 & 0 & 0 & 0 & 0 & 0 & \left(\frac{F_i k_{Pci}}{L_{fi}}\frac{\partial i_{qij}}{\partial v_{odj}}\right) & \left(\frac{F_i k_{Pci}}{L_{fi}}\frac{\partial i_{qij}}{\partial v_{oqj}}\right)\\
\frac{-1}{C_{fi}}\frac{\partial i_{dij}}{\partial \delta_j} & 0 & 0 & 0 & 0 & 0 & 0 & 0 & 0 & \frac{-1}{C_{fi}}\frac{\partial i_{dij}}{\partial v_{odj}} & \frac{-1}{C_{fi}}\frac{\partial i_{dij}}{\partial v_{oqj}}\\
\frac{-1}{C_{fi}}\frac{\partial i_{qij}}{\partial \delta_j} & 0 & 0 & 0 & 0 & 0 & 0 & 0 & 0 & \frac{-1}{C_{fi}}\frac{\partial i_{qij}}{\partial v_{odj}} & \frac{-1}{C_{fi}}\frac{\partial i_{qij}}{\partial v_{oqj}}
\end{bmatrix}$$

APPENDIX B
VSI's SMALL-SIGNAL MODEL

The VSI small signal model includes inner control loops, as shown in Fig. A.1, and LC filter.

Voltage control loop: the state variables of voltage control loop are defined as:

$$\dot{\phi}_{di}=v_{odrefi}-v_{odi} \quad \& \quad \dot{\phi}_{qi}=v_{oqrefi}-v_{oqi} \tag{A-1}$$

where v_{odrefi} and v_{oqrefi} are defined by the droop control in (13), and v_{odi} and v_{oqi} are the d-q components of measured output voltage, and index i denotes i^{th} DG unit. The voltage control loop's outputs are reference values for the current control loop as the following:

$$i_{fdrefi}=F_i\,i_{odi}-\omega_0\,C_{fi}v_{oqi}+k_{Pvi}\,\dot{\phi}_{di}+k_{Ivi}\,\phi_{di} \tag{A-2}$$

$$i_{fqrefi}=F_i\,i_{oqi}+\omega_0\,C_{fi}\,v_{odi}+k_{Pv}\,\dot{\phi}_{qi}+k_{Ivi}\,\phi_{qi} \tag{A-3}$$

where k_{Pv} and k_{Iv} are the proportional and integrator gains of the PI controller, respectively, see Fig. A.1(a).

Current control loop: the state variables of current control loop

are defined as:

$$\dot{\gamma}_{di} = i_{fdrefi} - i_{fdi} \quad \& \quad \dot{\gamma}_{qi} = i_{fqrefi} - i_{fqi} \tag{A-4}$$

where i_{fdrefi} and i_{fqrefi} are defined by the voltage control loop and i_{fdi} and i_{fqi} are the measured signals. The current control loop's outputs are reference values for the PWM unit as the following:

$$v_{Idiref} = -\omega_0 L_{fi}\, i_{fqi} + k_{Pci}\,\dot{\gamma}_{di} + k_{Ici}\,\gamma_{di} + v_{odi} \tag{A-5}$$

$$v_{Iqrefi} = \omega_0 L_{fi}\, i_{fdi} + k_{Pci}\,\dot{\gamma}_{qi} + k_{Ici}\,\gamma_{qi} + v_{oqi} \tag{A-6}$$

where k_{Pc} and k_{Ic} are the proportional and integrator gains of the PI controller, respectively, see Fig. A.1(b).

LC filter: after applying the Park transformation to the KVL and KCL equations obtained from the electrical circuit of the LC filter, the corresponding state variables are developed as:

$$\dot{i}_{fdi} = -\frac{R_{fi}}{L_{fi}} i_{fdi} + \omega_0 i_{fqi} + \frac{1}{L_{fi}} v_{Idrefi} - \frac{1}{L_{fi}} v_{iod} \tag{A-7}$$

$$\dot{i}_{fqi} = -\frac{R_{fi}}{L_{fi}} i_{fqi} - \omega_0 i_{fdi} + \frac{1}{L_{fi}} v_{Iqrefi} - \frac{1}{L_{fi}} v_{oqi} \tag{A-8}$$

$$\dot{v}_{odi} = \omega_0 v_{oqi} + \frac{1}{C_{fi}} i_{fdi} - \frac{1}{C_{fi}} i_{odi} \tag{A-9}$$

$$\dot{v}_{oqi} = -\omega_0 v_{odi} + \frac{1}{C_{fi}} i_{fqi} - \frac{1}{C_{fi}} i_{oqi} \tag{A-10}$$

where R_{fi}, L_{fi}, and C_{fi} are the resistance, inductance and capacitance of LC filter respectively, i_{fdi} and i_{fqi} are *d-q* components of the LC filter inductance currents, respectively, i_{odi} and i_{oqi} are d-q components of the output current of i^{th} bus.

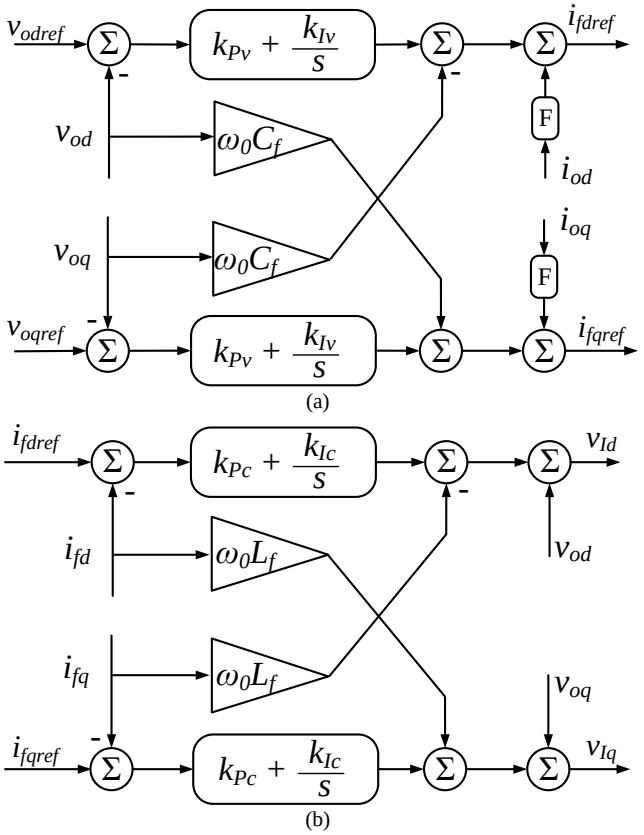

Fig. A.1. VSI's inner control loops: (a) voltage control loop; (b) current control loop.

Table A.I. Electrical and control parameters of VSI

LC filter	R_f	L_f	C_f
	0.1 Ω	1e-3 H	50e-6 F
Voltage control loop	k_{Pv}	k_{Iv}	F
	0.5	390	0.75
Current control loop	k_{Pc}	k_{Ic}	-
	10.5	16000	-
Power converter	Switching frequency	Rated power	Voltage (L-L)
	8 kHz	30 kW	400 V

REFERENCES

[1] D. E. Olivares *et al.*, "Trends in microgrid control," *IEEE Trans. on Smart Grid*, vol. 5, no. 4, pp. 1905-1919, 2014.

[2] M. H. Moradi, M. Eskandari, and S. M. Hosseinian, "Operational strategy optimization in an optimal sized smart microgrid," *IEEE Trans. on Smart Grid*, vol. 6, no. 3, pp. 1087-1095, 2015.

[3] J. M. Guerrero, J. C. Vasquez, J. Matas, L. G. De Vicuña, and M. Castilla, "Hierarchical control of droop-controlled AC and DC microgrids—A general approach toward standardization," *IEEE Trans. on Industrial Electronics*, vol. 58, no. 1, pp. 158-172, 2011.

[4] J. Rocabert, A. Luna, F. Blaabjerg, and P. Rodriguez, "Control of power converters in AC microgrids," *IEEE Trans. on Power Electronics*, vol. 27, no. 11, pp. 4734-4749, 2012.

[5] M. H. Moradi, M. Eskandari, and S. M. Hosseinian, "Cooperative control strategy of energy storage systems and micro sources for stabilizing microgrids in different operation modes," *International Journal of Electrical Power & Energy Systems*, vol. 78, pp. 390-400, 2016.

[6] T. L. Vandoorn, B. Meersman, L. Degroote, B. Renders, and L. Vandevelde, "A control strategy for islanded microgrids with dc-link voltage control," *IEEE Trans. on Power Delivery*, vol. 26, no. 2, pp. 703-713, 2011.

[7] M. S. Golsorkhi and D. D. Lu, "A control method for inverter-based islanded microgrids based on VI droop characteristics," *IEEE Trans. on Power Delivery*, vol. 30, no. 3, pp. 1196-1204, 2015.

[8] M. S. Golsorkhi and D. D.-C. Lu, "A decentralized control method for islanded microgrids under unbalanced conditions," *IEEE Trans. on Power Delivery*, vol. 31, no. 3, pp. 1112-1121, 2016.

[9] J. M. Guerrero, J. Matas, L. G. de Vicuna, M. Castilla, and J. Miret, "Decentralized control for parallel operation of distributed generation inverters using resistive output impedance," *IEEE Trans. on Industrial Electronics*, vol. 54, no. 2, pp. 994-1004, 2007.

[10] S.-J. Ahn, J.-W. Park, I.-Y. Chung, S.-I. Moon, S.-H. Kang, and S.-R. Nam, "Power-sharing method of multiple distributed generators considering control modes and configurations of a microgrid,"*IEEE Trans. on Power Delivery*, vol. 25, no. 3, pp. 2007-2016, 2010.

[11] Y. W. Li and C.-N. Kao, "An accurate power control strategy for power-electronics-interfaced distributed generation units operating in a low-voltage multibus microgrid," *IEEE Trans. on Power Electronics*, vol. 24, no. 12, pp. 2977-2988, 2009.

[12] J. M. Guerrero, J. C. Vasquez, J. Matas, M. Castilla, and L. G. de Vicuna, "Control strategy for flexible microgrid based on parallel line-interactive UPS systems," *IEEE Trans. on Industrial Electronics*, vol. 56, no. 3, pp. 726-736, 2009.

[13] J. Kim, J. M. Guerrero, P. Rodriguez, R. Teodorescu, and K. Nam, "Mode adaptive droop control with virtual output impedances for an inverter-based flexible AC microgrid," *IEEE Trans. on Power Electronics*, vol. 26, no. 3, pp. 689-701, 2011.

[14] J. He, Y. W. Li, J. M. Guerrero, F. Blaabjerg, and J. C. Vasquez, "An islanding microgrid power sharing approach using enhanced virtual impedance control scheme," *IEEE Trans. on Power Electronics*, vol. 28, no. 11, pp. 5272-5282, 2013.

[15] C. K. Sao and P. W. Lehn, "Control and power management of converter fed microgrids," *IEEE Trans. on Power Systems*, vol. 23, no. 3, pp. 1088-1098, 2008.

[16] M. Eskandari, L. Li, and M. H. Moradi, "Decentralized Optimal Servo Control System for Implementing Instantaneous Reactive Power Sharing in Microgrids," *IEEE Trans. on Sustainable Energy*, vol. 9, no. 2, pp. 525-537, 2018.

[17] C. A. Cortes, S. F. Contreras, and M. Shahidehpour, "Microgrid topology planning for enhancing the reliability of active distribution networks," *IEEE Trans. on Smart Grid*, vol. 9, no. 6, pp. 6369-6377, 2018.

[18] Z. Li, M. Shahidehpour, F. Aminifar, A. Alabdulwahab, and Y. Al-Turki, "Networked microgrids for enhancing the power system resilience,"

Proceedings of the IEEE, vol. 105, no. 7, pp. 1289-1310, 2017.

[19] Y. Zhu, F. Zhuo, F. Wang, B. Liu, R. Gou, and Y. Zhao, "A virtual impedance optimization method for reactive power sharing in networked microgrid," *IEEE Trans. on Power Electronics*, vol. 31, no. 4, pp. 2890-2904, 2016.

[20] J. W. Simpson-Porco, Q. Shafiee, F. Dörfler, J. C. Vasquez, J. M. Guerrero, and F. Bullo, "Secondary frequency and voltage control of islanded microgrids via distributed averaging," *IEEE Trans. on Industrial Electronics*, vol. 62, no. 11, pp. 7025-7038, 2015.

[21] L.-Y. Lu and C.-C. Chu, "Consensus-based droop control synthesis for multiple DICs in isolated micro-grids," *IEEE Trans. on Power Systems*, vol. 30, no. 5, pp. 2243-2256, 2015.

[22] J. Schiffer, T. Seel, J. Raisch, and T. Sezi, "Voltage stability and reactive power sharing in inverter-based microgrids with consensus-based distributed voltage control," *IEEE Trans. on Control Systems Technology*, vol. 24, no. 1, pp. 96-109, 2016.

[23] H. Zhang, S. Kim, Q. Sun, and J. Zhou, "Distributed adaptive virtual impedance control for accurate reactive power sharing based on consensus control in microgrids," *IEEE Trans. on Smart Grid*, vol. 8, no. 4, pp. 1749-1761, 2017.

[24] F. Guo, C. Wen, J. Mao, Y. D. Song, "Distributed secondary voltage and frequency restoration control of droop-controlled inverter-based microgrids," *IEEE Trans. on industrial Electronics*, vol. 62, no. 7, pp. 4355-4364, 2015.

[25] Y. Han, K. Zhang, H. Li, E. A. A. Coelho, and J. M. Guerrero, "MAS-based distributed coordinated control and optimization in microgrid and microgrid clusters: A comprehensive overview," *IEEE Trans. on Power Electron.*, vol. 33, no. 8, pp. 6488-6508, 2017.

[26] N. Pogaku, M. Prodanovic, and T. C. Green, "Modeling, analysis and testing of autonomous operation of an inverter-based microgrid," *IEEE Trans. on Power Electronics*, vol. 22, no. 2, pp. 613-625, 2007.

[27] A. Elrayyah, Y. Sozer, and M. E. Elbuluk, "A novel load-flow analysis for stable and optimized microgrid operation," *IEEE Trans. on Power Delivery*, vol. 29, no. 4, pp. 1709-1717, 2014.

[28] M. M. A. Abdelaziz, "Effect of detailed reactive power limit modeling on islanded microgrid power flow analysis," *IEEE Trans. on Power Systems*, vol. 31, no. 2, pp. 1665-1666, 2016.

[29] E. A. A. Coelho et al., "Small-Signal Analysis of the Microgrid Secondary Control Considering a Communication Time Delay," *IEEE Trans. on Industrial Electronics*, vol. 63, no. 10, pp. 6257-6269, 2016.

[30] M. Eskandari and L. Li, "A novel small signal model of multi-bus microgrids for modeling interaction of droop controllers through the power network," in *2017 20th International Conference on Electrical Machines and Systems (ICEMS)*, 2017, pp. 1-6: IEEE.

[31] E. H. Mamdani, S. Assilian. "An experiment in linguistic synthesis with a fuzzy logic controller." *International journal of man-machine studies*, vol. 7, no. 1, pp. 1-13, 1975.

[32] M. Eskandari and L. Li, "Microgrid operation improvement by adaptive virtual impedance," *IET Renewable Power Generation*, vol. 13, no. 2, pp. 296-307, 2018.

[33] M. Eskandari, L. Li, and M. H. Moradi, P. Siano. F. Blaabjerg, "Active Power Sharing and frequency Restoration in an Autonomous Networked Microgrids," *IEEE Trans. on Power Systems*, 2019.

[34] V. L. Syrmos, C. T. Abdallah, P. Dorato, and K. Grigoriadis, "Static output feedback—a survey," *Automatic*a, vol. 33, no. 2, pp. 125-137, 1997.

[35] Y.-Y. Cao, J. Lam, and Y.-X. Sun, "Static output feedback stabilization: an ILMI approach," *Automatica*, vol. 34, no. 12, pp. 1641-1645, 1998.

[36] L. E. Ghaoui, F. Oustry, M. AitRami. "A cone complementarity linearization algorithm for static output-feedback and related problems." *IEEE Trans. on Automatic Control*, vol. 42, no. 8, pp. 1171-1176, Aug 1997.

[37] J. Lofberg, "YALMIP: A toolbox for modeling and optimization in MATLAB," in *2004 IEEE international conference on robotics and automation (IEEE Cat. No. 04CH37508)*, 2004, pp. 284-289: IEEE.